Article

Acoustic and Dynamic Response of Unbaffled Plates of Arbitrary Shape

Pablo García-Fogeda [1,*] **, Fernando de la Iglesia** [2] **and Keyvan Salehi** [1]

1   Department of Aircraft and Space Vehicles, ETSIAE, Universidad Politécnica de Madrid, 28040 Madrid, Spain;
    keyvan.salehi@upm.es
2   Technology Department, Altran Innovación S.L., 28022 Madrid, Spain;
    fernando.delaiglesiamoreno@capgemini.com
*   Correspondence: pablo.garciafogeda@upm.es

Featured Application: The paper may be an excellent tool for treating the acoustic behaviour of arbitrary plate shapes and the response to diffuse acoustic fields. The integration scheme used to solve the Helmholtz equation is robust and efficient when compared to other existing methods.

Abstract: In this study, a method for determining the effects of fluids on the dynamic characteristics of an aerospace structure and the response of the structure when it is excited by the acoustical loads produced during a rocket launch, has been developed. Elevated acoustical loads are critical in the design of large lightweight structures, such as solar arrays and communication reflectors, because of the high acceleration levels. The acoustic field generated during rocket launch can be considered as a diffuse field composed of many uncorrelated incident plane waves traveling in different directions, which impinge on the structure. A boundary element method was used to calculate the pressure jump produced by an incoming plane wave on an unbaffled plate and the fluid–structure coupled loads generated through plate vibration. This method is based on Kirchhoff's integral formulation of the Helmholtz equation for pressure fields. The generalized force matrix attributed to the fluid loads was then formulated, taking the modes of the plate in vacuum as base functions of the structural displacement. These modes are obtained using a finite-element model. An iteration procedure was developed to calculate the natural frequencies of the fully coupled fluid–plate system. Comparison of the results obtained using the proposed method with those of other theories and experimental data demonstrated its efficiency and accuracy. The proposed method is suitable for analyzing plates of arbitrary shape subjected to any boundary conditions in a diffuse field for low to medium values of the frequency excitation range.

1. Introduction

Spacecraft structures, such as communication reflectors and solar arrays, are excited by an intense acoustic field during launcher lift-off. The acceleration levels induced by the acoustic loads can be very high, because of the very low densities of these structures. Acoustic loads can damage sensitive parts of a structure and the electronic equipment attached to it. Therefore, light aerospace structures are subjected to intense acoustic tests in large reverberant chambers. The aerospace industry requires a method to predict the acceleration levels reached when the acoustic loads excite these structures. Therefore, the catastrophic damage that occurs when acoustic tests are performed in the reverberant chamber can be prevented during the design phase.

Two effects need to be considered when the dynamic response of the structure under acoustic loads is investigated: Plate radiation and external sources generated acoustic wave

diffraction when the loads impinge on the structure. These effects are coupled and thus produce continuous feedback between the structural and acoustic behaviors.

The dynamic behavior of these types of structures has recently received attention from several investigators. Therefore, the stress level and concentration for glass fiber reinforced polimer composites has been studied by Ferdous et al. [1] and the behaviour under impact loads by Zangana et al. [2] and He et al. [3].

The problem of coupling between a baffled plate and an acoustic field has been investigated extensively, e.g., Berry et al. [4], Filippi et al. [5], Lomas and Hayek [6], Stepanishen [7], Skudrzyk [8], Wu et al. [9] and Sharma and Sarkar [10,11]. Unbaffled plates have been studied recently because of some additional difficulties identified by Atalla et al. [12], Gascón and García-Fogeda. [13], Nelisse et al. [14], Laulagnet [15], and Nowak and Zielinski [16]. For all cases examined in this study, the plate is assumed to be unbaffled.

The effect of the surrounding air on the dynamic characteristics of these types of structures cannot be ignored. There may be significant differences between the analysis and vibration tests, owing to the presence of air. Therefore, the effect of the surrounding air must be considered during the modeling to validate mathematical models of structural dynamics. A fluid (including a light fluid, such as air) influences the natural frequency, damping coefficient, and normal modes when the structure is made of a very low-density material. Fowler et al. [17], Maidanik [18], Arenas [19], and Mattei [20] provided some examples of this phenomenon. The assumption of light coupling cannot be applied therefore for this case.

For complex structures, the governing equations of the fluid–structure interaction must be solved numerically. Among the different numerical techniques, the boundary element method (BEM) and the finite element method (FEM) are the most widely used to solve this type of problem. The advantages of the BEM for solving a vibrating plate surrounded by the fluid include the satisfaction of the far-field radiation conditions and the relatively low number of discretization elements. However, the main disadvantage is that the matrix of influence coefficients is complete with no zeros. Therefore, the BEM method is more expensive than the FEM method in solving a linear system of equations where the matrix has a bandwidth diagonal. Ben Mariem and Hamdi [21], Coyette [22], Göranson et al. [23], and Nowak and Zielinski [16] used the BEM/FEM model to solve acoustical problems. In relation to the use of FEM models for solving acoustic problems, there are several commercial software programs based on this method. Among them, it is worth mentioning COMSOL Multiphysics, whose acoustic module allows modeling acoustic propagation problems in both solids and fluids (see for example, Gieva et al. [24]). Both the FEM and the BEM are only valid for low- to medium-frequency ranges to solve fluid-structure interaction problems. For high-frequency ranges, a method such as statistical energy analysis (SEA) must be used (e.g., Paolozzi and Peroni, [25]).

Troclet et al. [26] and ESA PSS-03-204 [27] showed that the acoustic lift-off noise of a launcher could be characterized as a diffuse field. Realistic modeling of the acoustic field must be conducted to reflect this loading effect on the response of the structure. Nelisse et al. [14] and Tseng [28] reported that a good representation of the diffuse field could be determined by superposing uncorrelated incident plane waves traveling throughout space. The direction of each plane wave was characterized by a pressure spectral density.

In this paper, a numerical method for solving a fully coupled fluid–structure problem is presented. The method can be used to analyze the effect of the surrounding fluid on the dynamic characteristics of the unbaffled plate of a trapezoidal planform and the response of the plate to a diffuse field. The method is based on a BEM for the fluid domain and a FEM for the structure. The plate can be subjected to any type of boundary conditions. The normal modes of the plate in vacuum are adopted as basis functions to determine plate deformation for the fully coupled fluid–structure. Therefore, the number of degrees of freedom of the structure is significantly reduced, as demonstrated by Grooteman et al. [29]. In the BEM numerical model, the plate is divided into trapezoidal elements, and on each

element, the pressure that jumps across the plate is assumed to be constant. The influence coefficient matrix is obtained through numerical integration, taking the finite part when the integral is singular using the Hadamard method. Numerical results are presented to demonstrate the robustness of the integration scheme of the method and are compared to results obtained using more sophisticated methods, such as the Hamdi functional approach (Hamdi and Jean, [30]).

The method developed is robust due to the integration scheme used and accounts for the strong coupling between compressible fluids and plates of any shape. The contribution of the fluid to the damping of the plate is also determined.

The response of the unbaffled rectangular plate to a diffuse field is determined using the proposed method and the RAYON code used by Hamdi [31]. The differences between the results obtained using the proposed method and RAYON are negligible. Other results, such as the effect of the surrounding air on the dynamic characteristics of rectangular and trapezoidal plates, are also presented in this paper. The physical transcendency of these results in terms of variation in the natural frequency and additional damping owing to the fluid is described.

2. Models and Methods

A flat, isotropic, homogeneous, thin plate of arbitrary shape and under any support condition is considered. The plate is in the $z = 0$ *plane* and one of its sides is selected as the *x*-axis (Figure 1).
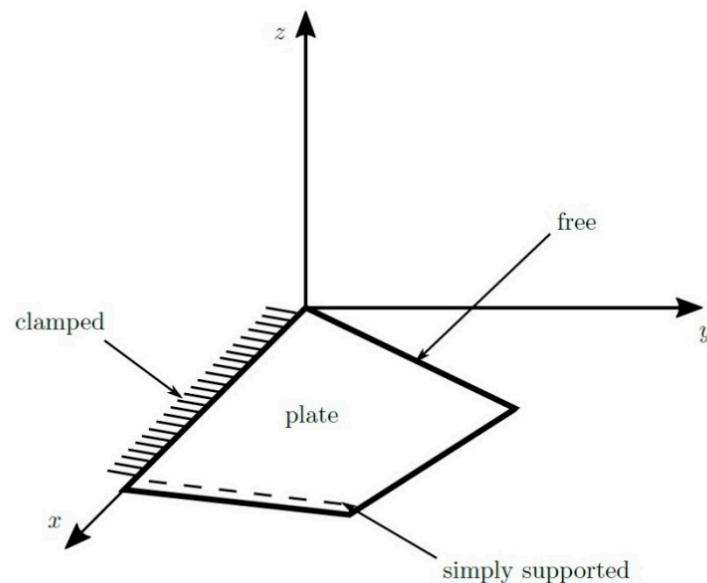

Figure 1. Example of plate.

The differential equation that governs the transverse displacement *w (x, y, t)* of the plate with constant thickness and without structural damping can be expressed as follows (Laulagnet, [15]):

$$D\nabla^4 w + \rho_M h \frac{\partial^2 w}{\partial t^2} = \Delta\widetilde{P}(x,y,t) + f(x,y,t) \tag{1}$$

where D is the flexural rigidity, ρ_M is the material density, h is the plate thickness, $\Delta\widetilde{P}$ is the acoustic pressure jump across the plate, surface, and $f(x,y,t)$ represents the external forces other than the forces exerted by the fluid. The equations for the plate are completed based on the boundary conditions at the edge of the plate.

The pressure jump $\Delta\widetilde{P}$ can be expressed as follows:

$$\Delta\widetilde{P}(x,y,t) = \Delta\widetilde{P}_{vib}(x,y,t) + \Delta\widetilde{P}_{wave}(x,y,t) \tag{2}$$

where $\Delta\widetilde{P}_{vib}$ is the pressure jump owing to the plate radiation, and $\Delta\widetilde{P}_{wave}$ is the pressure jump owing to the load induced by the incident plane wave over its surface when the plate is rigid. It is assumed that small perturbations occur in a compressible, inviscid and irrotational fluid, and these pressure distributions can be calculated by solving the wave equation for the fluid domain, expressed as follows:

$$\nabla^2 p - \frac{1}{a_\infty^2}\frac{\partial^2 p}{\partial t^2} = 0 \tag{3}$$

where a_∞ is the speed of sound in the fluid at rest.

The application of the momentum equation at the plate surface yields the following boundary condition:

$$\frac{\partial p}{\partial z} = -\rho_\infty\frac{\partial^2 w}{\partial t^2} \quad \text{at } z = \pm 0 \tag{4}$$

where ρ_∞ is the fluid density.

At an extended distance from the plate, the Sommerfeld radiation condition must be satisfied. It is assumed that the motion is harmonic for both the fluid and the structure to solve the system of Equations (1), (3) and (4). Therefore, the transverse displacement $w(x,y,t)$ and pressure $p(x,y,z,t)$ can be written as follows.

$$w(x,y,t) = W(x,y)e^{-i\omega t}$$

$$p(x,y,z,t) = P(x,y,z)e^{-i\omega t} \tag{5}$$

The deformation of the plate $W(x,y)$ can be expressed as a linear combination of the normal modes of the plate in vacuum, which are determined using the FEM model. Let these modes be $W_m(x_j,y_j)$, where (x_j,y_j) are the coordinates of the FEM model nodes. An analytical expression valid for all (x,y) for the plate is obtained through curve fitting in a Lagrange polynomial form. The deformation of the plate is then derived as follows:

$$w(x,y,t) = \sum_{m=1}^{M}\sum_{n=1}^{N} q_{mn}^0 W_{mn}(x,y)e^{-i\omega t} \tag{6}$$

where the q_{mn}^0 are unknown coefficients to be determined when the coupled fluid–structure equations are solved, and $W_{mn}(x,y)$ are the curve-fitted modes. The modes of the plate in vacuum are chosen as a basis, and the number of degrees of freedom can be significantly reduced.

Next, the independent variables x, y, and z are nondimensionalized using the plate characteristic length l_c, which is defined as $l_c = \sqrt{S_p}$, where S_p is the plate area.

2.1. Calculation of Pressure Jump $\Delta\widetilde{P}_{wave}$

For harmonic motion, the pressure generated by a plane wave in directions θ and ϕ at any point in the space can be expressed as follows (Nelisse et al. [14]):

$$P_i(x,y,z) = P_0 e^{-ik(\sin\phi\cos\theta + \sin\phi\sin\theta + z\cos\phi)} \tag{7}$$

where $k = \omega/a_\infty$ is the acoustic wave number.

The pressure field (the sum of the incident plane wave field and the diffracted field) must satisfy Equation (3) and the following boundary condition at the plate surface when the plate is considered perfectly rigid:

$$\frac{\partial P}{\partial z} = 0 \quad \text{at } z = \pm 0 \ \text{ in } S_p \tag{8}$$

By applying Green's theorem, the equation for the pressure field can be written as follows:

$$P(x,y,z) = P_i(x,y,z) + \frac{1}{4\pi} \iint_{S_p} \Delta\widetilde{P}_{wave}(\xi,\eta) \frac{\partial}{\partial z}\left(\frac{e^{-ikR}}{R}\right) d\xi d\eta \tag{9}$$

where

$$\Delta\widetilde{P}(\xi,\eta) = \lim_{\epsilon \to 0}[P(\xi,\eta,-\epsilon) - P(\xi,\eta,+\epsilon)] \tag{10}$$

and $\frac{e^{-ikR}}{R}$ is the free space Green function.

After the boundary condition, Equation (8), is applied, the following integral equation for calculating $\Delta\widetilde{P}_{wave}$ is derived:

$$ik\cos\phi P_0 e^{ik\sin\phi(\cos\theta x + \sin\theta y)} = -\frac{1}{4\pi} \iint_{S_p} \Delta\widetilde{P}_{wave}(\xi,\eta) \frac{\partial^2}{\partial z^2}\left(\frac{e^{-ikR}}{R}\right)\Bigg|_{z=0} d\xi d\eta \tag{11}$$

2.2. Calculation of Pressure Jump $\Delta\widetilde{P}_{vib}$

Radiated pressure generated by plate vibration can be expressed as a double layer distribution on the plate surface (Capitaine and Lome, [32]; Putra and Thompson, [33]). Applying Green s theorem for a pure harmonic motion, it is possible to express Equation (2) as a distribution of dipoles on the plate surface (Maidanik, [18]):

$$P(x,y,z) = -\frac{1}{4\pi} \iint_{S_p} \Delta\widetilde{P}_{vib}(\xi,\eta) \frac{\partial}{\partial z}\left(\frac{e^{-ikR}}{R}\right) d\xi d\eta \tag{12}$$

The boundary conditions are applied to the surface of the plate, and Equation (13) is derived to determine the pressure jump across the plate:

$$\frac{\partial P(x,y,z)}{\partial z}\Bigg|_{z=0} = \rho_\infty\omega^2 \sum_{m=1}^{M}\sum_{n=1}^{N} q_{mn}^0 W_{mn}(x,y) = -\frac{1}{4\pi} \iint_{S_p} \Delta\widetilde{P}_{vib}(\xi,\eta) \frac{\partial^2}{\partial z^2}\left(\frac{e^{-ikR}}{R}\right)\Bigg|_{z=0} d\xi d\eta \tag{13}$$

Due to the linearity of Equation (13), the pressure jump $\left(\Delta\widetilde{P}_{vib}\right)_{mn}$ for each plate deformation mode W_{mn} is obtained.

2.3. Boundary Element Method

The integral equation (13) is solved as follows. First, the plate is divided into panels (of trapezoidal/triangular shape), as depicted in Figure 2. The numbers of panels are set as I in the x-direction and J in the y-direction. Therefore, $I \cdot J$ is the total number of panels. The pressure in each panel is assumed to be constant and therefore the "jump" in pressure at panel ij is equal to $\left(\Delta\widetilde{P}_{mn}\right)_{ij}$ due to the normal mode W_{mn}. The integral on the surface of the plate is then evaluated as the sum of all panels, resulting in the following expression:

$$q_{mn}^0 \rho_\infty\omega^2 l_c W_{mn}(x,y) = -\frac{1}{4\pi} \sum_{i=1}^{I}\sum_{j=1}^{J}\left(\Delta\widetilde{P}_{vib(mn)}\right)_{ij} \iint_{S_{pij}} \frac{\partial^2}{\partial z^2}\left(\frac{e^{-ikR}}{R}\right)\Bigg|_{z=0} d\xi d\eta \tag{14}$$
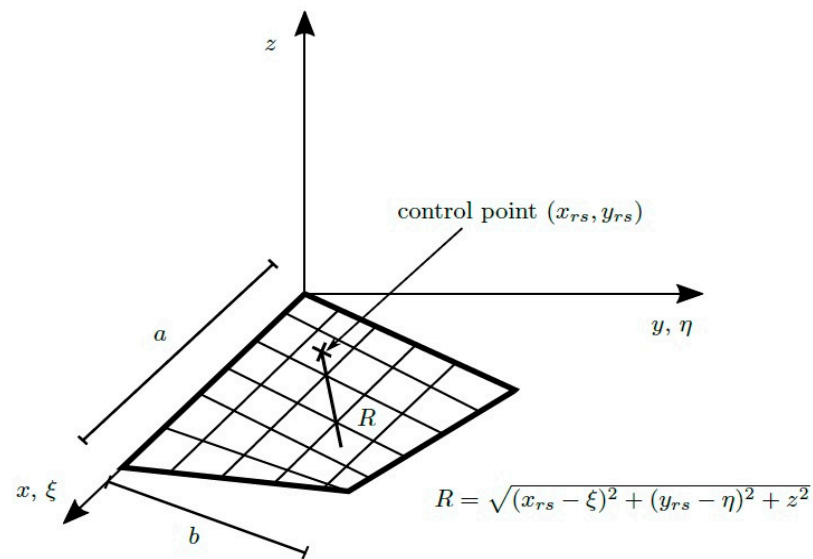
Figure 2. Division of plate into elements.

The integral equation at $I \cdot J$ control points located at the geometric center of each panel is satisfied to obtain a linear system of $I \cdot J$ equations for the pressure jump distribution (either $\Delta \widetilde{P}_{vib}$) associated with the mode W_{mn}.

Condition (14) may be represented in a matrix form as:

$$[AIC]\left\{\Delta \widetilde{P}\right\}_{mn} = -4\pi\rho_\infty \omega^2 l_c q^0_{mn}\{W_{mn}\} \tag{15}$$

where the influence coefficients of the matrix $[AIC]$ are defined as follows:

$$AIC^{rs}_{ij} = \iint\limits_{S_{pij}} \frac{\partial^2}{\partial z^2}\left(\frac{e^{-ikR}}{R}\right)\bigg|_{z=0} d\xi d\eta \tag{16}$$

In the integral expressed in Equation (16), special care must be taken for the singularity that occurs when the element of integration coincides with the element where the boundary condition is satisfied. Let the integrand be established as follows.

$$K(x_{rs} - \xi, y_{rs} - \eta) = K(x_0, y_0) \tag{17}$$

The singular part of function is added and subtracted to prevent numerical instabilities. Therefore, the integral can be expressed as follow:

$$\iint K(x_0, y_0)dx_0 dy_0 = \iint [K(x_0, y_0) - K_s(x_0, y_0)]dx_0 dy_0 + F.P. \iint K_s(x_0, y_0)dx_0 dy_0 \tag{18}$$

The first integral on the right side is no longer singular when $x_0 \to 0$ and $y_0 \to 0$, and it can be evaluated numerically. The second integral can be analytically evaluated, and the finite part in Hadamard s sense can be used. The robustness of the integration method is validated using the following example. For very low frequencies, function $K_s(x_0, y_0)$ can be expanded in the form of Taylor series, as follows:

$$K_s(x_0, y_0) \approx -\frac{1}{R^3} - \frac{k^2}{2R} + \frac{ik^3}{3} \tag{19}$$

If a rectangular element of sides 2a and 2b is considered, the integration of the expanded form of the function K_s, that is, Equation (19), after the finite part of the integral of the term, $1/R^3$, is selected, yields the following expression:

$$\frac{-4\sqrt{a^2+b^2}}{ab} - \frac{k^2}{2}4b\ln\left|\frac{a+\sqrt{a^2+b^2}}{b}\right| - \frac{k^2}{2}4a\ln\left|\frac{b+\sqrt{a^2+b^2}}{ba}\right| + \frac{ik^3}{3}(4ab) \quad (20)$$

The results obtained using Equation (20) are compared with the numerical procedure described for evaluating the integrals in Equation (18) and Figure 3. Both methods are in excellent agreement, and the slight difference was attributed to the number of terms used in the Taylor series expansion. As the procedure for evaluating the integral in Equation (18) is independent of the nondimensional frequency k, the above results demonstrate the robustness of the integration method. The method described to treat the singularity provides accurate results (see Figure 3). Although other methods, such as the ones given by Nowak and Zielinski [16] and Hamdi and Jean [30], for example, are equally effective for treating this singularity.
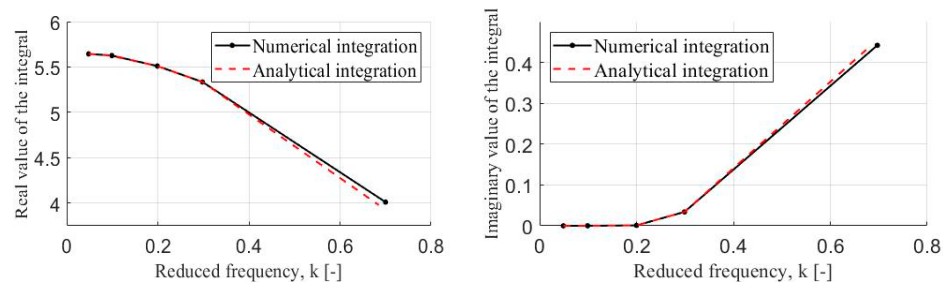
Figure 3. Comparison of numerical and exact integration of singular terms of the kernel for low frequencies.

The same procedure is used to solve the integral Equation (9), adopted as the unknown parameter at panel ij $\left(\Delta\widetilde{P}_{wave}\right)_{ij}$:

After all pressure distributions have been calculated, the generalized force for the uvth mode is evaluated:

$$Q_{uv} = \iint\limits_{S_p} \Delta\widetilde{P}W_{uv}d\sigma = \iint\limits_{S_p} \Delta\widetilde{P}_{vib}W_{uv}d\sigma + \iint\limits_{S_p} \Delta\widetilde{P}_{wave}W_{uv}d\sigma \quad (21)$$

The equations of motion for the generalized coordinates associated with the modes of plate vibration, including the forces exerted by the plane wave, can then be expressed as follows:

$$\left(-\omega^2[\mathbb{M}] + [\mathbb{K}]\right)\{q\} = \{Q\} = \left[Q_{mn}^{vib}\right]\{q\} + \{Q^{wave}\} = \omega^2[\mathbb{M}]_f\{q\} + \{Q^{wave}\} \quad (22)$$

where $[\mathbb{M}]$ is the structural mass matrix, $[\mathbb{K}]$ is the structural rigidity matrix, and $[\mathbb{M}]_f$ is the fluid mass matrix. The solution of this linear system results in the vector $\{q\}$. This vector represents the participation factor of the vacuum modes in the total response of the fluid-loaded plate to an incident wave.

Equation (22) can be rearranged and expressed as follows:

$$\left(-\omega^2\left([\mathbb{M}] + [\mathbb{M}]_f\right) + [\mathbb{K}]\right)\{q\} = \{Q^{wave}\} \quad (23)$$

If no external forces are considered, except those generated by the surrounding fluid due to the free vibration of the plate, the resultant homogeneous system will induce the natural frequencies and normal modes of the coupled fluid–structure system.

2.4. Procedure for Computing Natural Frequencies

The natural frequencies of the system are determined by making the determinant formed by the two mass matrices and the stiffness matrix equal to zero. However, the added mass matrix $[\mathbb{M}]_f$ depends on the oscillation frequency of the plate, and thus, an iteration procedure must be applied. The developed iteration scheme can be simplified in the following steps:

The natural frequencies of the system are computed, assuming that the surrounding fluid is incompressible.

1. A set of reduced frequencies is then determined, defined as $k_j = \frac{\omega_{j,\,incompr} \cdot l_c}{a_\infty}$, where ωj is the jth natural frequency of the coupled incompressible fluid structure.
2. These results are assumed as an initial guess, and by letting the added mass matrix to now be a function of k, the natural frequencies of the system are recalculated until convergence is achieved (for further details, see Gascón and García-Fogeda [8]). For each natural frequency, the procedure converges after two or three iterations. For a compressible fluid, the natural frequencies are obtained sequentially, whereas for an incompressible fluid, all natural frequencies are obtained simultaneously.
3. After the natural frequencies of the coupled fluid–structure system have been determined, the normal modes can be computed and expressed as a linear combination of the normal modes of the structure in vacuum.

2.5. Calculation of the Dynamic Response of the Structure Immersed in the Diffuse Field

A diffuse field can be modeled by superpositioning plane waves traveling in different directions (Nelisse et al. [14]; Kim et al. [34]; Capitaine and Lome, [32]; Tseng [28]. Let us assume that the elemental power spectral density of the incident wave in the ij direction, defined by angles θ and ϕ (Figure 4), is $W_{p_{ij}}(\omega)$ (in Pa^2/Hz). If the different directions of the incident waves are uncorrelated, the total power spectral density $\hat{W}_\mathrm{P}$ will be the sum of all the elemental densities. As the acoustic requirement of a launcher is expressed in N dB per octave for a specific bandwidth (ESA PSS-03-204, [27]), the total power spectral density W_p is constant over such a bandwidth, which results in the following expression:

$$N = 10\log \frac{P2}{P_r^2} = 10\log \frac{\hat{W}_p \Delta f}{P_r^2} \tag{24}$$

where $Pr = 2 \times 10^{-5}$ Pa is the reference pressure. From Equation (24), the power spectral density equation can be written as follows:

$$\hat{W}_p = \frac{P_r^2}{\Delta f} 10^{N/10} \tag{25}$$
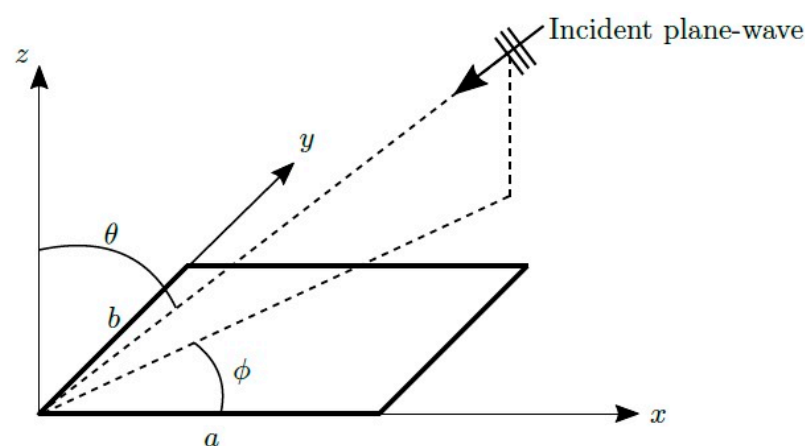

Figure 4. Geometrical representation of the unbaffled plate submitted to plane wave.

The space field is divided into a finite number of directions θ_i and φ_j. There is a solid angle a_{ij} associated with each direction. It is assumed that the power spectral density in the *ij* direction is $a_{ij} \cdot \hat{W}_p(\omega)$, where $\hat{W}_p$ is the total power spectral density.

When all problem parameters have been defined, the structural response to the diffuse field is obtained as follows.

Let $H_{r_{ij}}(\omega)$ be the transfer function between the *r* degree of freedom of the structure and the plane wave in the *ij* direction. The power spectral density induced by all plane waves in the solid angle corresponding to the *ij* direction for the *r*th degree of freedom is obtained using Equation (26):

$$\hat{W}_{r,ij} = \left| H_{r,ij}(\omega) \right|^2 \hat{W}_{pij} = \left| H_{r,ij}(\omega) \right|^2 a_{ij} \hat{W}_p \tag{26}$$

As all directions are uncorrelated, it can be demonstrated that for a random field, the structural response is obtained as the sum of the elemental spectral densities (Nigam and Narayanan, [35]):

$$\hat{W}_r(\omega) = \hat{W}_p(\omega) \sum_{i,j} \left| H_{r,ij}(\omega) \right|^2 a_{ij} \tag{27}$$

Thus, the relationship between the power spectral density of the *r* degree of freedom of the structure, the acoustic power spectral density W_p, and the transference function between the *r* degree of freedom and the plane waves consisting of the diffuse field is established.

3. Results

3.1. Acoustic Loading on a Rigid Plate

Diffraction of a plane wave impinging on a rigid plate is considered to validate the code. The results obtained are compared with those of the semi-analytical method developed by Nelisse et al. [14]. The orientations of the incident plane wave are $\theta = 0°$ and $\phi = 0°$ (i.e., perpendicular to the plate), and the amplitude is unity. Figure 5 shows the absolute values of the sound pressure jump at the point $(0.27, 0.3)$ in the panel as a function of the frequency range between 0 and 500 Hz. The results show excellent agreement between the predictions of both methods. As the influence coefficient matrix is common for the calculated pressure jump of both rigid and vibrating plates, the code used to calculate the natural frequencies is validated.
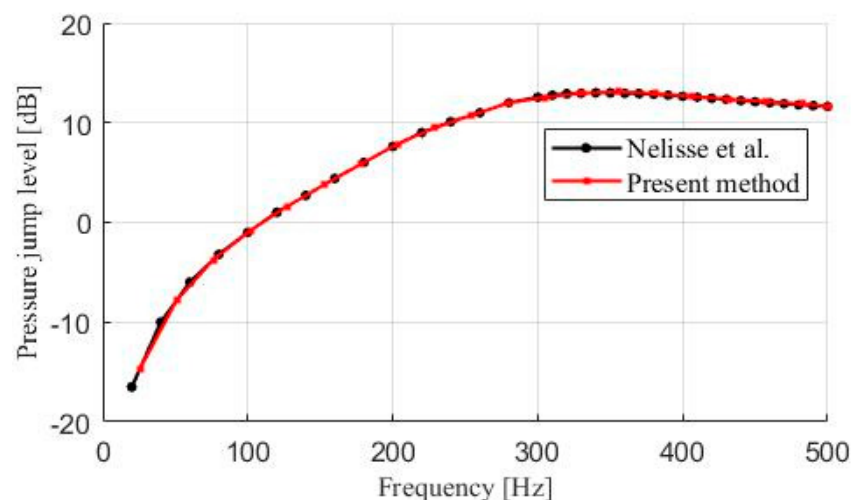
Figure 5. Pressure jump across a rigid plate at a point.

3.2. Effect of Fluid on Dynamic Plate Characteristics

Next, the effect of the surrounding fluid on the dynamic characteristics of the plate is investigated. The cases considered are a rectangular simply supported plate, and trape-

zoidal simply supported and cantilever plates. Table 1 lists the first four values of natural frequency for the cases of no fluid, incompressible fluid, and compressible fluid. All plates were of sandwich type, and the acoustic medium surrounding the plates was air. The material properties and thickness of these plates were as follows: $E = 4.41 \times 10^9$ N/m^2, $\upsilon = 0.29$, $h = 15.78 \times 10^{-3}$ m, and $\rho_M = 130.7$ kg/m^3.

Table 1. Natural frequency and equivalent damping values for rectangular and trapezoidal plates.

	Rectangular Simply Supported Plate			
	Frequency (Hz)			Equivalent Damping (kg/s)
	In vacuum	Incompressible	Compressible	
1st mode	563.1	525.5	540.8	262.1
2nd mode	1006.4	961.6	1000.0	514.8
3rd mode	1482.0	1432.9	1479.2	143.9
4th mode	1701.0	1647.9	1699.6	180.2
	Trapezoidal Plate Simply Supported			
	Frequency (Hz)			Equivalent Damping (kg/s)
	In vacuum	Incompressible	Compressible	
1st mode	168.2	148.7	142.9	26.1
2nd mode	350.3	324.8	309.1	11.2
3rd mode	448.2	418.8	410.9	215.1
4th mode	622.2	592.1	604.8	183.4
	Trapezoidal Cantilever Plate			
	Frequency (Hz)			Equivalent Damping (kg/s)
	In vacuum	Incompressible	Compressible	
1st mode	27.5	24.9	24.9	0.01
2nd mode	84.5	79.5	79.3	1.12
3rd mode	147.2	133.6	133.5	0.14
4th mode	245.1	232.3	229.9	1.87

This type of structure is used in the aerospace industry because it is light and stiff. For such structures, the fluid effects are very significant. The dimensions of the rectangular plate are 0.6 m $\times$ 0.386 m, and the trapezoidal plate has a base of 1 m, a short base of 0.6 m, and a height of 1 m.

As expected, it can be observed that the natural frequencies of the plates decrease from the vacuum values. With respect to the support condition, it is noticed that this effect is more significant for the simply supported plate than for the cantilever plate, which signifies that the added mass value of the first plate is higher than that of the second plate. The reduction in natural frequency decreases with increasing modal order. Arenas obtained similar findings [19]. With respect to the plate shape, a stronger reduction in the natural frequencies is observed for the trapezoidal plate than for the rectangular plate for the same boundary conditions.

In Figures 6–8, the real and imaginary parts of the added mass matrix for the three plates versus the nondimensional frequency are presented. With these figures, we want to observe how the real part affects the natural frequencies and how the imaginary part does it to the damping coefficient, for the plates investigated. For all cases, the value of the added mass increases from the incompressible case ($k = 0$) until it reaches a maximum, and then decreases toward zero. If the nondimensional frequency of the mode in vacuum is located before the maximum, the natural frequencies are reduced owing to the fluid. However, the frequencies tend to reach the vacuum value if the nondimensional frequency is located after the maximum. With respect to the imaginary part of the added mass matrix, it is observed that for any reduced frequency these terms are always positive, showing that the fluid influence for these cases is always stabilizing. In relation to the real part of the added mass, there is a minimum value and then tend towards the value of zero,

showing that, at very high frequencies, the contribution of the fluid is very small and can be neglected.
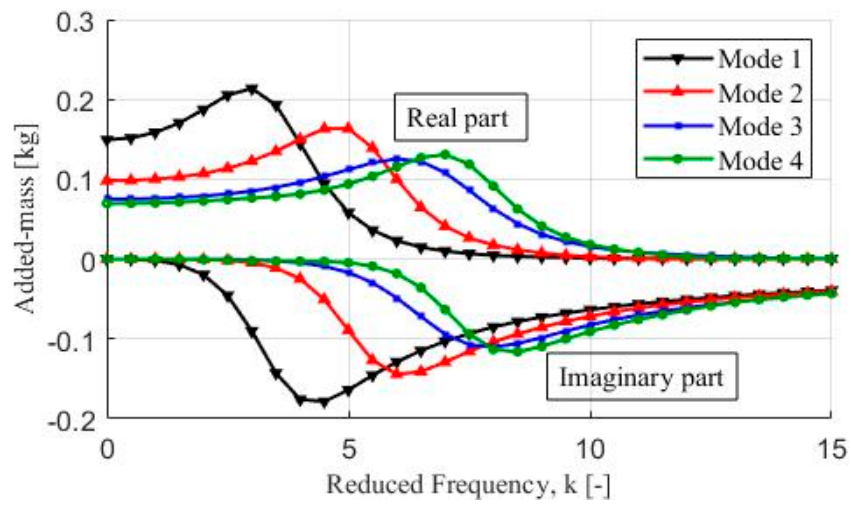

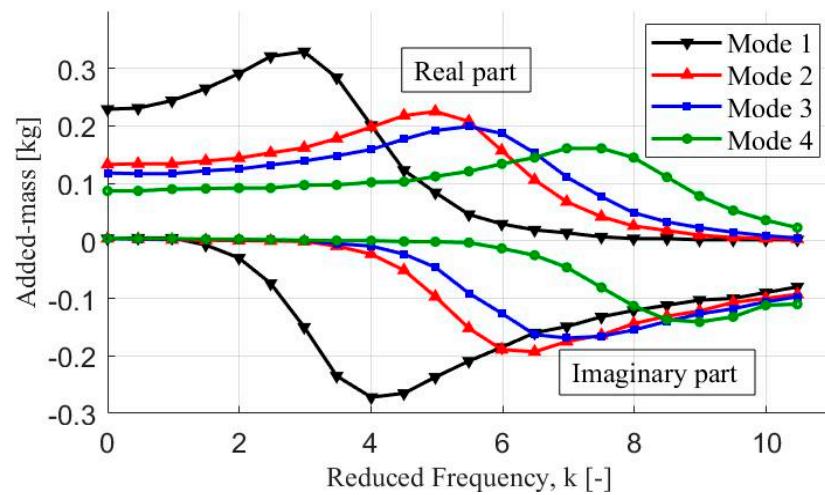**Figure 6.** Added mass terms as function of reduced frequency of rectangular simply supported plate.

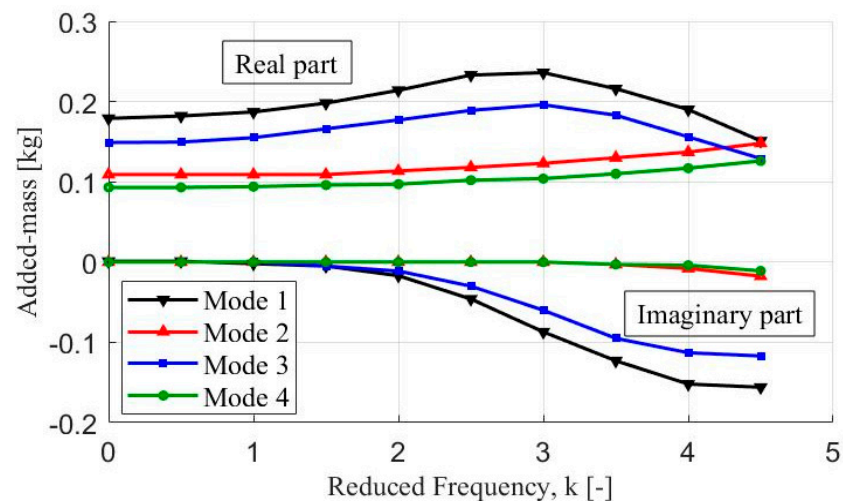**Figure 7.** Added mass terms as function of reduced frequency for trapezoidal simply supported plate.

Figure 8. Added mass terms as a function of reduced frequency for the trapezoidal cantilever plate.

Figures 9–11 show the fluid damping ratio $\gamma = -\frac{m_i \omega}{C_{cr}}$, where m_i is the imaginary part of the diagonal terms of the added mass matrix for each mode, and C_{cr} is the critical damping of the corresponding mode. Perhaps, the most interesting result is the equivalent fluid damping for the first mode of the trapezoidal cantilever plate. The ratio of the equivalent damping coefficient to the system critical damping coefficient (corresponding to this mode) reaches a peak value of 0.95. When this value is compared to the empirical value (0.2) typically used in design analysis, it could be difficult to predict these values correctly when the fluid is considered. It may be true that in most cases, the equivalent damping of the fluid, which tends to have a constant value (as observed in Figures 9–11), does not exceed 0.2. However, it has been demonstrated that such an approach may be unrealistic in some cases.
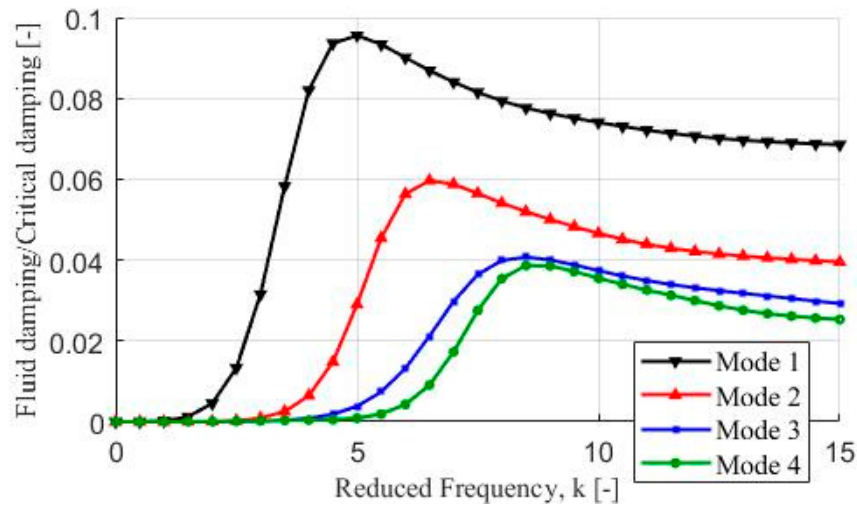

Figure 9. Fluid damping ratio as function of reduced frequency for rectangular simply supported plate.
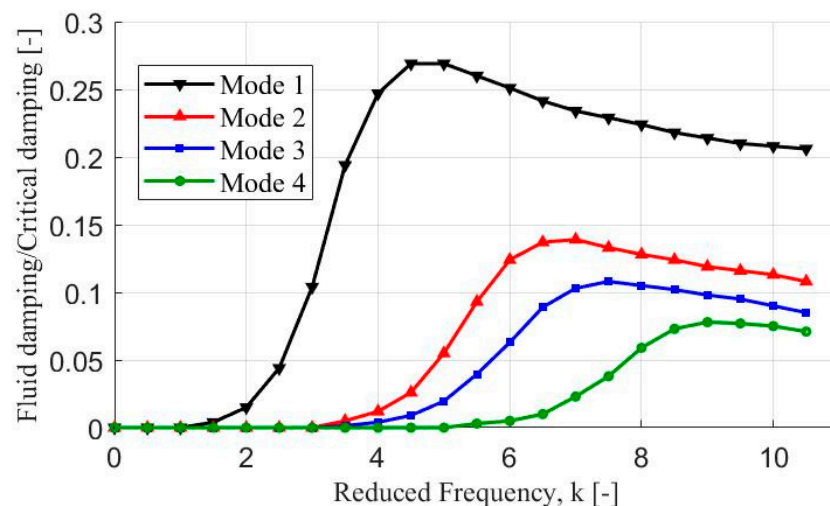

Figure 10. Fluid damping ratio as function of reduced frequency for trapezoidal simply supported plate.
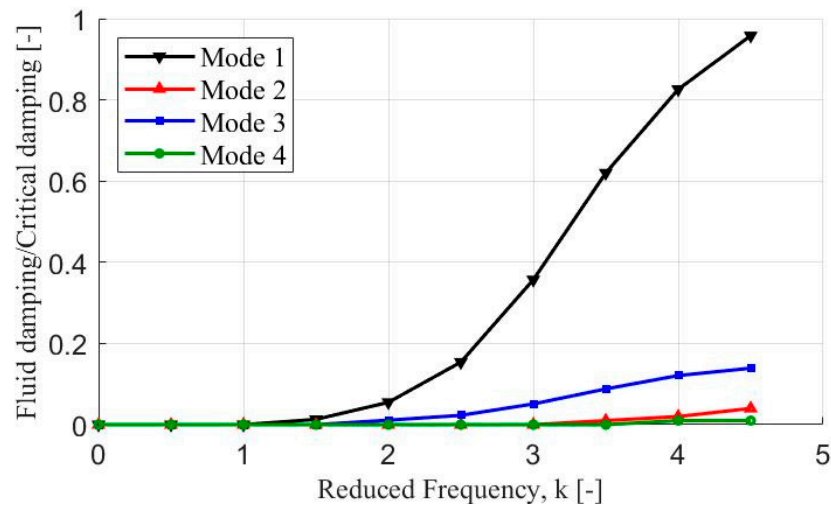
Figure 11. Fluid damping ratio as a function of reduced frequency for cantilever trapezoidal plate.

3.3. Response of a Rectangular Plate to the Diffuse Field

Consider a rectangular plate of 0.386 m × 0.6 m under free–free support conditions with the following structural characteristics: $E = 9 \times 10^9$ N/m^2, $\upsilon = 0.30$, $h = 16 \times 10^{-3}$ m, and $\rho_M = 129$ kg/m^3.

For this plate, the response to a diffuse field was computed. The numerical results obtained using the proposed method were compared (Figures 12–14) with those obtained using a computer code RAYON (Hamdi, [31]). The results of both numerical methods were in good agreement at a frequency range of 0–1400 Hz, but different BEM models were established in both methods: Direct formulation and variable approach.
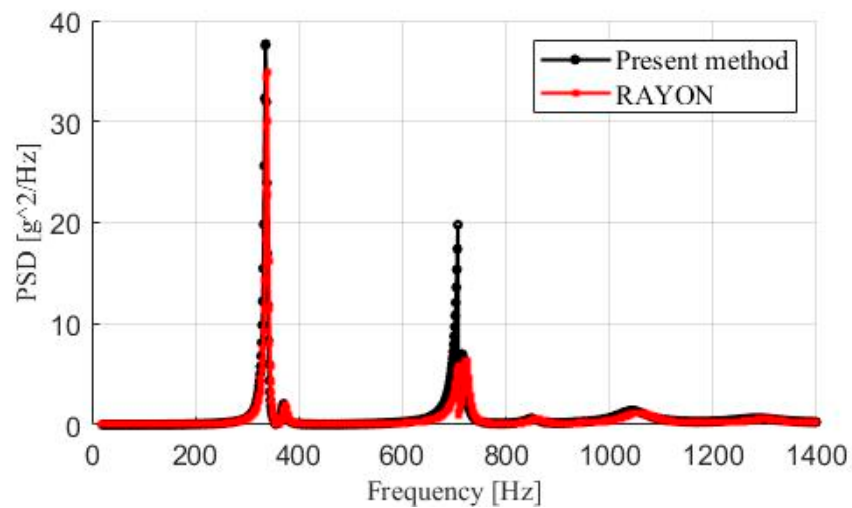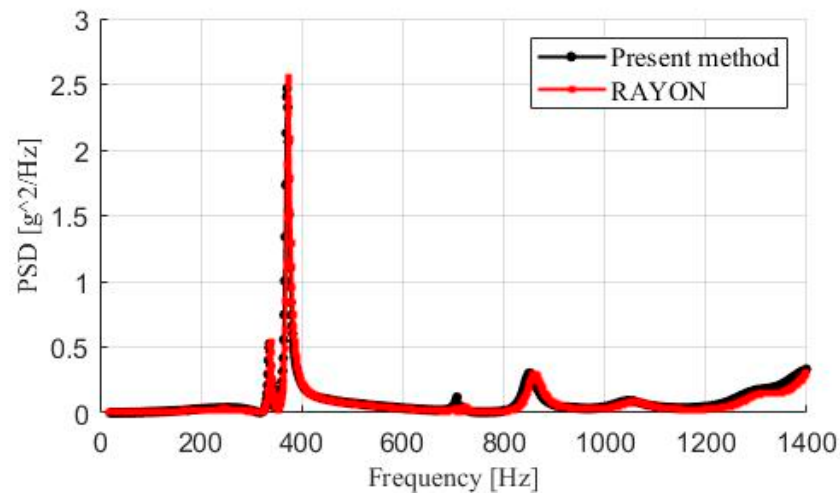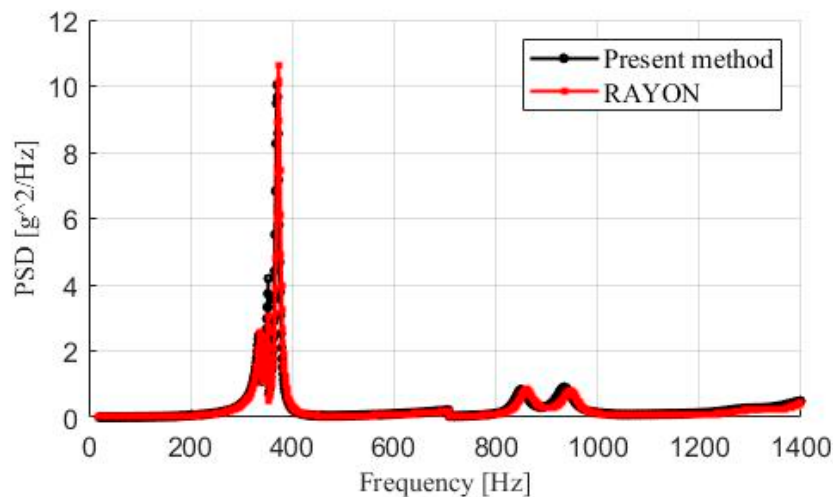

Figure 12. Power spectral density at node P1X (0.0, 0.386) for rectangular plate immersed in diffuse field.

Figure 13. Power spectral density at node P2X (0.3, 0.208) for rectangular plate immersed in diffuse field.

Figure 14. Power spectral density at node P3X (0.6,0.208) for a rectangular plate immersed in a diffuse field.

The inference from this comparison is that the proposed method is as robust as other well-established methods. The proposed method can analyze complex geometries and be fully compatible with structural codes, such as NASTRAN.

4. Conclusions

In this study, a method of determining the dynamic characteristics of a plate immersed in a diffuse field under different support conditions for low- to medium-frequency frequencies was developed. The numerical integration procedure of the kernel function was validated using existing data and the proposed method showed excellent efficiency and accuracy. The reduction of the natural frequencies of a sandwich plate due to the surrounding fluid has been calculated. The added mass and fluid damping modal coefficients were described in physical terms as a function of the reduced frequency, and it was demonstrated that their effects could not be neglected in dynamic calculations.

The response of the rectangular plate to a diffuse field was determined and compared to that of RAYON. The numerical results were in excellent agreement with those obtained using RAYON. Further investigations should be conducted for the diffuse field using another model.

A robust method for fully coupling of a compressible fluid and a plate has been presented. The method has the capability to predict the influence of the fluid on the

dynamic characteristics of the plate surrounded by the fluid, and to determine the response of the coupled fluid structure to external loadings.

A promising application of our method would be to space structures, such as antennas or solar panels, dynamically tested on earth (surrounded by air) and operating in vacuum. With the proposed method, the effect of air, when the structure is tested, can be subtracted, thereby improving the dynamical model of the system.

Author Contributions: Conceptualization, P.G.-F. and F.d.l.I.; methodology, P.G.-F.; software, F.d.l.I.; validation, F.d.l.I.; formal analysis, P.G.-F. and K.S.; investigation, P.G.-F. and F.d.l.I.; resources, P.G.-F. and F.d.l.I.; data curation, F.d.l.I. and K.S.; writing—original draft preparation, P.G.-F. and K.S.; writing—review and editing, P.G.-F. and K.S.; visualization, K.S.; supervision, P.G.-F. and K.S. All authors have read and agreed to the published version of the manuscript.

Institutional Review Board Statement: Not applicable.

Informed Consent Statement: Not applicable.

Data Availability Statement: Not applicable.

Conflicts of Interest: The authors declare no conflict of interest.

References

1. Ferdous, W.; Manalo, A.; Peauril, J.; Salih, C.; Reddy, K.R.; Yu, P.; Schubel, P.; Heyer, T. Testing and modelling the fatigue behaviour of GFRP composites—Effect of stress level, stress concentration and frequency. *Eng. Sci. Technol. Int. J.* **2020**, *23*, 1223–1232. [CrossRef]
2. Zangana, S.; Epaarachchi, J.; Ferdous, W.; Leng, J.; Schubel, P. Behaviour of continuous fibre composite sandwich core under low-velocity impact. *Thin-Walled Struct.* **2020**, *158*, 107157. [CrossRef]
3. He, W.; Liu, J.; Wang, S.; Xie, D. Low-velocity impact response and post-impact flexural behaviour of composite sandwich structures with corrugated cores. *Compos. Struct.* **2018**, *189*, 37–53. [CrossRef]
4. Berry, A.; Guyader, J.; Nicolas, J. A general formulation for the sound radiation from rectangular, baffled plates with arbitrary boundary conditions. *J. Acoust. Soc. Am.* **1990**, *88*, 2792–2802. [CrossRef]
5. Filippi, P.; Lagarrigue, O.; Mattei, P.-O. Perturbation Method for Sound Radiation By A Vibrating Plate In A Light Fluid: Comparison With The Exact Solution. *J. Sound Vib.* **1994**, *177*, 259–275. [CrossRef]
6. Lomas, N.S.; Hayek, S.I. Vibration and acoustic radiation of elastically supported rectangular plates. *J. Sound Vib.* **1977**, *52*, 1–25. [CrossRef]
7. Stepanishen, P.R. The radiation impedance of a rectangular piston. *J. Sound Vib.* **1977**, *55*, 275–288. [CrossRef]
8. Skudrzyk, E. *The Foundations of Acoustics*; Springer: Berlin/Heidelberg, Germany, 1971; ISBN 3211809880. [CrossRef]
9. Wu, H.; Jiang, W.; Liu, Y. Analyzing Acoustic Radiation Modes of Baffled Plates with a Fast Multipole Boundary Element Method. *J. Vib. Acoust.* **2013**, *135*, 011007. [CrossRef]
10. Sharma, G.S.; Sarkar, A. Directivity based control of acoustic radiation. *Appl. Acoust.* **2019**, *154*, 226–235. [CrossRef]
11. Sharma, G.S.; Sarkar, A. Directivity-Based Passive Barrier for Local Control of Low-Frequency Noise. *J. Theor. Comput. Acoust.* **2018**, *26*, 1850012. [CrossRef]
12. Atalla, N. Acoustic radiation of an unbaffled vibrating plate with general elastic boundary conditions. *J. Acoust. Soc. Am.* **1996**, *99*, 1484–1494. [CrossRef]
13. Gascón-Pérez, M.; Garcia-Fogeda, P. Induced Damping on Vibrating Circular Plates Submerged in Still Fluid. *Int. J. Appl. Mech.* **2015**, *7*, 1550079. [CrossRef]
14. Nélisse, H.; Beslin, O.; Nicolas, J. Fluid–structure coupling for an unbaffled elastic panel immersed in a diffuse field. *J. Sound Vib.* **1996**, *198*, 485–506. [CrossRef]
15. Laulagnet, B. Sound radiation by a simply supported unbaffled plate. *J. Acoust. Soc. Am.* **1998**, *103*, 2451–2462. [CrossRef]
16. Nowak, L.J.; Zieliński, T.G. Determination of the Free-Field Acoustic Radiation Characteristics of the Vibrating Plate Structures with Arbitrary Boundary Conditions. *J. Vib. Acoust.* **2015**, *137*, 051001. [CrossRef]
17. Fowler, J.; Lagerquist, N.; Leve, H. Effect of Air in Modal Tests. In Proceedings of the 5th International Modal Analysis Conference, London, UK, 6–9 April 1987.
18. Maidanik, G. Response of Ribbed Panels to Reverberant Acoustic Fields. *J. Acoust. Soc. Am.* **1962**, *34*, 809–826. [CrossRef]
19. Arenas, J.P. On the vibration analysis of rectangular clamped plates using the virtual work principle. *J. Sound Vib.* **2003**, *266*, 912–918. [CrossRef]
20. Mattei, P.-O. A Two-Dimensional Tchebycheff Collocation Method for The Study of The Vibration of A Baffled Fluid-Loaded Rectangular Plate. *J. Sound Vib.* **1996**, *196*, 407–427. [CrossRef]

21. Ben Mariem, J.; Hamdi, M.A. A new boundary finite element method for fluid-structure interaction problems. *Int. J. Numer. Methods Eng.* **1987**, *24*, 1251–1267. [CrossRef]
22. Coyette, J.P. A Synthesis of Available Numerical Methods for Modeling Vibroacoustic Problem. In Proceedings of the Congress Spacecraft Structures and Mechanical Testing, Paris, France, 21–24 June 1994.
23. Göransson, P.; Ek, K.; Brandt, J.; Defosse, H.; Hamdi, M.A.; Mebarek, L.; Faust, M.; Baier, H.; Klein, M.; Witting, M. New Coupled Finite Element and Boundary Element Approaches to Perform 3-Dimensional Payload Effect Simulations in Launcher Payloads Compartment Structures. In Proceedings of the Congress Spacecraft Structures and Mechanical Testing, CNES/ESA, Paris, France, 21–24 June 1994, ISSN 0766-1002.
24. Gieva, E.E.; Ruskova, I.N.; Nedlchev, K.I.; Kralov, I. COMSOL Numerical Investigation of Acoustic Absorber. In Proceedings of the IX National Conference with International Participation Conference "Electronica 2018", Sofia, Bulgaria, 17–18 May 2018. [CrossRef]
25. Paolozzi, A.; Peroni, I. Response of aerospace sandwich panels to launch acoustic environment. *J. Sound Vib.* **1996**, *196*, 1–18. [CrossRef]
26. Troclet, B.; Vanpeperstraete, S.; Schott, M. Experimental Analysis of Lift-off and Aerodynamic Noise on the Ariane 5 Launch Vehicle. In Proceedings of the First Joint CEAS/AIAA Aeroacoustics Conference, Munich, Germany, 12–15 June 1995; pp. 535–544.
27. ESA PSS-03-204. *Structural Acoustics Design Manual*; ESA Publication Division, ESTEC: Noordwijk, The Netherlands, 1996; Issue 1; ISSN 0379-4059.
28. Tseng, W.-K. A Novel Method of Designing Quiet Zones in Diffuse Fields. *J. Vib. Acoust.* **2013**, *135*, 011001. [CrossRef]
29. Grooteman, F.P.; de Boer, A.; Schippers, H. Vibro-Acoustic Analysis of Double Wall Structures. In Proceedings of the First Joint CEAS/AIAA Aeroacoustics Conference, Munich, Germany, 12–15 June 1995; pp. 1049–1054.
30. Hamdi, M.A.; Jean, P. A Mixed Functional for the Numerical Resolution of Fluid-Structure Interaction Problems. In *Aero- and Hydro-Acoustics*; Comte-Bellot, G., Williams, J.E.F., Eds.; IUTAM Symposia (International Union of Theoretical and Applied Mechanics); Springer: Berlin/Heidelberg, Germany, 1986.
31. Hamdi, M.A. *RAYON User's Manual*; STRACO S.A.: Compiegne, France, 1992.
32. Capitaine, A.; Lome, J.-M. Prediction de la Response Dynamique d'une Structure dans un Champ Acoustique Diffus. Correlation avec des Test. In Proceedings of the Congress Spacecraft Structures and Mechanical Testing, Paris, France, 21–24 June 1994.
33. Putra, A.; Thompson, D. Radiation efficiency of unbaffled and perforated plates near a rigid reflecting surface. *J. Sound Vib.* **2011**, *330*, 5443–5459. [CrossRef]
34. Kim, M.J.; Won, K.S.; Ri, C.S. An Improved MSA Model for Evaluating the Sound Transmission Loss of a Rectangular Plate for a Diffuse Field Incidence. *Arch. Acoust.* **2019**, *44*, 259–265.
35. Nigam, N.C.; Narayanan, S. *Applications of Random Vibrations*; Springer: Berlin/Heidelberg, Germany; Narosa Publishing House: New Delhi, India, 1994; ISBN 354019861X.